Transverse modulational dynamics of quenched patterns

Sierra Dunn, 1 Ryan Goh, 2, a) and Benjamin Krewson²

(Dated: 2 May 2024)

We study the modulational dynamics of striped patterns formed in the wake of a planar directional quench. Such quenches, which move across a medium and nucleate pattern-forming instabilities in their wake, have been shown in numerous applications to control and select the wavenumber and orientation of striped phases. In the context of the prototypical complex Ginzburg-Landau and Swift-Hohenberg equations, we use a multiple-scale analysis to derive a one-dimensional viscous Burgers' equation which describes the long-wavelength modulational and defect dynamics in the direction transverse to the quenching motion, that is along the quenching line. We show that the wavenumber selecting properties of the quench determines the nonlinear flux parameter in the Burgers' modulation equation, while the viscosity parameter of the Burgers' equation is naturally determined by the transverse diffusivity of the pure stripe state. We use this approximation to accurately characterize the transverse dynamics of several types of defects formed in the wake, including grain boundaries and phase-slips.

Directional quenching is a novel way to harness selforganized pattern-forming processes in a variety of systems. Here an external mechanism rigidly progresses across a medium, exciting pattern-forming instabilities in its wake. While recent work has sought to understand how the orientation and wavenumber of striped patterns are selected by the quench, little has been done to understand the dynamics of defects and modulations of such patterns. Focusing on the interfacial dynamics of the patterned front just behind the quench, we derive a viscous Burgers' modulation equation to understand slowly-varying modulational dynamics in the direction perpendicular, or transverse, to the quenching motion. Crucially, we find that the selected wavenumber in the direction of quenching motion determines the parameters of the viscous Burgers' equation. We evidence the ubiquity of this modulational approximation by characterizing several types of wavenumber defects in quenched versions of the prototypical Complex Ginzburg-Landau and Swift-Hohenberg equations.

I. INTRODUCTION

Directional quenching has arisen as a novel way to harness, mediate, and control pattern forming instabilities in diverse application areas. Generally, some sort of external mechanism, possibly controlled by the experimenter, travels across the domain initiating a pattern-forming instability in its wake. One then hopes to control the shape, size, and orientation of the pattern by altering the speed and structure of the quench. Some examples include ramped fluid flows (Ref. 1), solidification problems in crystal formation (Ref. 2), and light-sensing reaction-diffusion experiments (Refs. 3 and 4). Additionally, directionally quenched systems serve as a proto-

type and testbed to understand how spatio-temporal heterogeneities and growth processes affect pattern-forming systems. Most works have studied the existence of stripe-forming front solutions in the wake of a quench, in particular focusing on how the quenching speed and shape affect the orientation and bulk wavenumber of the far-field pattern. Furthermore, a few works have studied (in)stability of these front solutions in specific systems (Ref. 5 and 6). See (Ref. 7 and 8) for recent reviews of these works as well as references to other application areas.

In comparison, relatively little is known about the dynamics, defects, and interactions of striped patterns formed in different sub-domains behind the quench. This becomes a question of interest, for example, when one studies the evolution of a quenched system starting with small fluctuations of the homogeneous background state. Here, patches of large amplitude patterns interact through defects which move along the quenching line. See for example Fig. 3 of the aforementioned (Ref. 3) or Fig. 2 of (Ref. 4). There a quench, while generally organizing the wavenumber and orientation of the local striped phase, still leaves behind several defects and imperfections which evolve as the quench moves through the system. See also, for example, Figure 1 below which depicts the evolution of the quenched domain from random perturbation of the trivial state in the complex Ginzburg-Landau equation. Motivated by such phenomena, we seek to understand and model defect dynamics in such quenched stripe formation.

This work considers quenched patterns in two spatial dimensions where the quench rigidly propagates in the horizontal direction. Previous works have shown that such quenches select the horizontal wavenumber k_x , and thus the temporal frequency ω , of the asymptotic pattern. In particular, they are determined by the quenching speed c and the transverse wavenumber k_y . We use a formal multiple-scales analysis to derive a reduced one-dimensional model for transverse modulations of striped patterns, that is we consider vertical modulations along the quenching line. As they determine the far-field pattern, we focus on solution dynamics just behind the quenching line. We show that a one-dimensional vis-

¹⁾Department of Mathematics and Statistics, Mount Holyoke College, 415A Clapp Laboratory, South Hadley, MA, 01075 USA;

²⁾Department of Mathematics and Statistics, Boston University, 665 Commonwealth Ave., Boston, MA 02215, USA:

a)rgoh@bu.edu

cous Burgers' equation accurately predicts the dynamics of slowly-varying, small amplitude wavenumber modulations. Most strikingly, we find that the selection of a unique horizontal wavenumber k_x for a given speed c determines the viscosity and nonlinear flux parameters in the associated viscous Burgers' equation. In Section II, we demonstrate our approach through asymmetric grain boundary and phase-slip examples in the prototypical complex Ginzburg Landau equation. In Section III, we then show its applicability in the Swift-Hohenberg equation, studying similar types of defects. We expect such modulation equations will predict transverse dynamics in many other quenched systems where the asymptotic pattern is diffusively stable (Ref. 9). While we mostly focus on transverse modulations of vertically independent stripes, with $k_v = 0$ so they are oriented parallel to the quench, we expect our results to apply to slowly-varying modulations of obliquely oriented stripes as well. Finally, in Section IV we discuss future directions and briefly propose a phenomenological boundary condition, derived from the selected wavenumber k_x as a function of k_y , to study quenched stripe modulations for the CGL equation using a fully two-dimensional nonlinear phase diffusion equation.

II. PROTOTYPICAL EXAMPLE: THE QUENCHED COMPLEX GINZBURG-LANDAU EQUATION

A. Quenched stripes

To introduce our approach, we consider the complex Ginzburg-Landau (CGL) equation (Ref. 10) with cubic supercritical nonlinearity, posed in the plane,

$$A_t = (1 + i\alpha)\Delta A + \chi(x - ct)A - (1 + i\gamma)A|A|^2$$

$$A \in \mathbb{C}, \quad (x, y) \in \mathbb{R}^2, \quad \alpha, \gamma \in \mathbb{R},$$

$$(1)$$

with directional quenching heterogeneity, $\chi(\xi) = -\mathrm{sign}(\xi)$, a step-function which rigidly propagates with speed $c \ge 0$ and which renders the trivial state A = 0, which is stable for x - ct > 0, into an unstable state for x - ct < 0. We transform into a co-moving frame of speed c in the horizontal direction, setting $\xi = x - ct$, to obtain

$$A_{t} = (1 + i\alpha)(\partial_{\xi}^{2} + \partial_{y}^{2})A + cA_{\xi} + \chi(\xi)A - (1 + i\gamma)A|A|^{2}.$$
(2)

Due to the invariance of the equation under the gauge action $A \mapsto e^{i\theta}A$, the homogeneous version of (2) with $\chi \equiv 1$ has explicit spatially periodic relative equilbria $A_p(\xi, y, t; k_x, k_y) = re^{i(k_x\xi + k_yy - \omega t)}$ with respect to this symmetry action. Furthermore, the amplitude r and wavenumber $k^2 = k_x^2 + k_y^2$ satisfies the following nonlinear dispersion relation in the co-moving frame

$$r^2 = 1 - k^2$$
, $\omega = (\alpha - \gamma)k^2 - ck_x + \gamma$. (3)

Once again due to the gauge invariance, the simplest stripe forming front solutions of (2) take the form

$$A(\xi, y, t) = e^{i(k_y y - \omega t)} A_f(\xi; c, k_y), \tag{4}$$

where A_f is a function of the co-moving frame variable ξ , c the quenching speed, and k_y the transverse wavenumber of the front. It solves the following traveling wave ODE with corresponding asymptotic boundary conditions

$$0 = (1 + i\alpha)(\partial_{\xi}^{2} - k_{y}^{2})A_{f} + cA_{f,\xi} + (\chi(\xi) + i\omega)A_{f} - (1 + i\gamma)A_{f}|A_{f}|^{2}, \quad (5)$$

$$0 = \lim_{\xi \to -\infty} \left| A_{\mathbf{f}}(\xi) - r e^{ik_x \xi} \right|, \qquad 0 = \lim_{\xi \to +\infty} A_{\mathbf{f}}(\xi), \tag{6}$$

for some horizontal wavenumber k_x . To summarize, A_f connects the stable trivial state ahead of the quench to a periodic pattern with horizontal wavenumber k_x . If a solution of (5)-(6) exists, one obtains a solution of the full PDE which connects a striped pattern with wavevector (k_x, k_y) to the trivial state ahead of the quench. The work (Ref. 11) rigorously established the existence of such fronts for $k_v = 0$ in the fast growth regime where $c \lesssim c_{\text{lin}} := 2\sqrt{1+\alpha^2}$, the linear spreading speed of fronts invading into the homogeneous unstable state for $\chi \equiv 1$ (Ref. 12). It showed that the temporal frequency ω , and thus the horizontal wavenumber k_x is determined, or "selected," by the quenching speed c, giving leading order expansions for this dependence. We denote these selected quantities as ω_f and $k_{x,f}$. Further, since the term involving k_y is a regular perturbation, we expect a family of front solutions, smoothly dependent on k_v^2 , to persist for $k_v \sim 0$. This means that (5)-(6) has a solution for an interval of k_v values containing 0 for each $c \in (0, c_{\text{lin}})$ fixed. Hence the frequency and horizontal wavenumber will also be selected by k_v^2 . In sum, these quantities can be written locally as graphs $\omega_f(c, k_v), k_{x,f}(c, k_v)$ over (c,k_y) -space; see Fig. 28 of (Ref. 8) for more discussion of these graphs. We denote the corresponding family of front solutions as $A_f(\xi; k_v, c)$. Figure 2 gives numerical continuation results using AUTO07p (Ref. 13) which continue fronts $A_{\rm f}$ and horizontal wavenumber $k_{x,{\rm f}}$ in both c and k_y for several values of α . We refer to the corresponding surface in (c, k_v, k_x) -space as the moduli space of quenched stripes (Ref. 8, §5.3) as it organizes which type(s) of stripes can be selected for a given quenching speed. The rigorous existence of such fronts for other values of c and $k_y \neq 0$ is the subject of current work.

For the remainder of the work we shall fix c > 0 such that a traveling-front solution of (5) exists for all k_y close to 0, and hence we suppress the dependence of c in our notation. We consider parameters α, γ such that stripes are Benjamin-Feir stable, $1 + \alpha \gamma > 0$. Substituting $k_{x,f}$ for k_x , the nonlinear dispersion relation then takes the form

$$\omega_{\rm f}(k_{\rm y}) = (\alpha - \gamma)(k_{\rm x,f}(k_{\rm y})^2 + k_{\rm y}^2) - ck_{\rm x,f}(k_{\rm y}) + \gamma.$$
 (7)

Since $k_{x,f}$ is smoothly dependent on k_y^2 , a simple calculation gives that both $\frac{\partial}{\partial k_y} k_{x,f}(0) = \frac{\partial}{\partial k_y} \omega_f(0) = 0$, yielding the expansion

$$k_{x,f}(k_y;c) = k_{x,f}(0) + \beta_2 k_y^2 + \mathcal{O}(k_y^4), \qquad k_y \sim 0,$$

for some constant β_2 . See Figure 2 for a depiction of this quadratic dependence near $k_y = 0$. As it will be critical in our

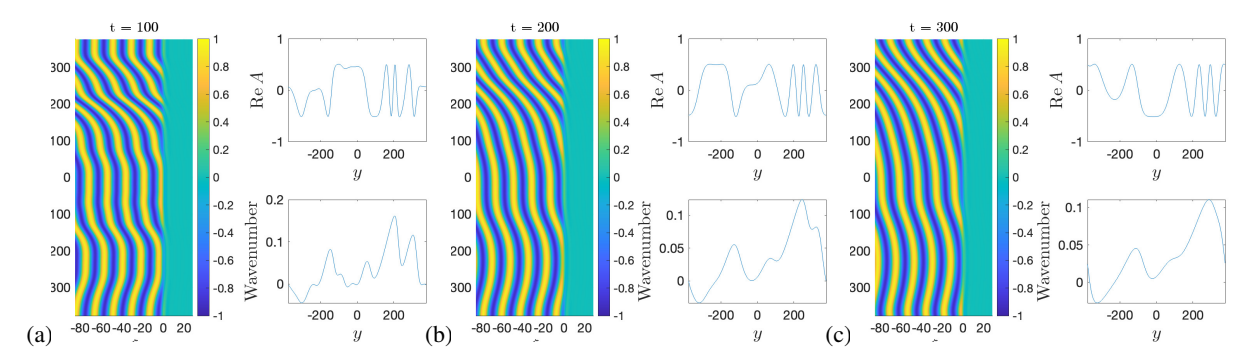


FIG. 1. Evolution of 2D quenched pattern in (2) in (ξ, y) variables, with $\alpha = 3, \gamma = 1, c = 2.5$, from small random initial data at times t = 100, 200, 300 (a) - (c) respectively, the co-moving frame with c > 0 causes stripes to emanate to the left from the quench line, note c > 0 corresponds to a right-ward traveling quenching line in the stationary frame; left subplots depict $\text{Re}A(\xi, y, t)$, upper right plots $\text{Re}A(\xi_0, y, t)$ for $\xi_0 = -1$, while lower right plots the measured local transverse wavenumber, calculated as $\text{Im} \frac{A_y}{A}$ for $\xi = \xi_0$ fixed.

modulation equation, we also calculate, recalling $\partial_{k_y} k_{x,\mathrm{f}}(0) = 0$, that

$$\partial_{k_{y}}^{2}\omega_{f}(0) = 2(\alpha - \gamma) + \partial_{k_{y}}^{2}k_{x,f}(0)(2(\alpha - \gamma)k_{x,f}(0) - c).$$
 (8)

The first term in (8) arises from standard 1-D modulational theory (Ref. 14) as concavity of the homogeneous dispersion relation (3). We highlight the second term as it is explicitly induced by the wavenumber selection caused by the quench. As will be seen in the following section, this will lead to an altered nonlinear flux coefficient; see (Ref. 14, Eqn. 3.17).

Initiating (2) from small random initial data with speed c=2.5, one observes the formation of patches of coherent stripes, oriented with weak oblique angle to the quench interface. One observes slow modulations in the striped phases as well as dislocation-like defects and grain boundaries of various orientations and angles; see Figure 1. Taking a cross-section in y for some $\xi_0 < 0$ just behind the quench location at $\xi=0$, one observes wavenumber dynamics similar to 1-D systems.

B. Transverse modulations

To study the dynamics of small amplitude, long wavenlegnth transverse modulations in the y-direction, we adapt the approach of (Ref. 14) which considers stripes in 1-D; see also (Ref. 10, §II.G). We look for slow transverse modulations of front solutions of (2) by introducing a slowly-varying transverse phase modulation function $\Phi(Y,T)$ dependent on the slow variables $Y = \delta y$, $T = \delta^2 t$ for some small parameter $0 < \delta \ll 1$, and form the ansatz

$$A(\xi,y,t) = \mathrm{e}^{\mathrm{i}(\Phi(Y,T) - \omega_{\mathrm{f}}t)} \left[A_{\mathrm{f}}(\xi;\delta\Phi_{Y}(Y,T)) + \delta^{2}w_{1}(\xi,Y,T;\delta) \right].$$

Here, $\Psi := \partial_Y \Phi$ gives the slowly-varying transverse wavenumber modulation and w_1 higher order corrections. We insert this ansatz into (2) and its associated complex-conjugate equation. We treat Y, T and y, t as independent variables. Note that while slow and fast variable derivatives formally do not commute, this has no effect in our case as A_f and the coefficients of (2) are independent of t and y. We then collect terms

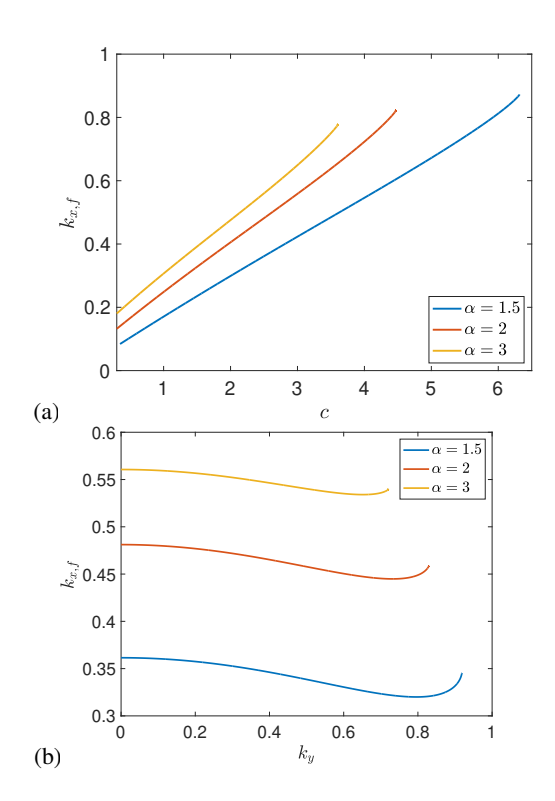


FIG. 2. Wavenumber selection curves with $\gamma=1$ and $\alpha=1.5,2,3$. Plot of the wavenumber selection curves $k_{x,f}$ against c for $k_y=0$ fixed (a), and against k_y for c=2.5 fixed (b). Note the quadratic behavior near $k_y=0$. In (a) note that the curves terminate at the linear spreading speed $c_{\text{lin}}=2\sqrt{1+\alpha^2}\approx 3.61,4.47$, and 6.33 respectively.

of the same order in δ , and fix $\xi = \xi_0$, a location just behind the quench with $-1 \le \xi_0 < 0$. At $\mathcal{O}(1)$ in δ we obtain the traveling wave equation (5) for the front, at $\mathcal{O}(\delta)$ we obtain an equation for the kernel of the associated linearized equation, satisfied by the derivative of the front solution along the gauge action, and finally at $\mathcal{O}(\delta^2)$ we obtain a linear equation in (w_1, \bar{w}_1) . The solvability condition for this equation yields the following viscous Burgers equation for the trans-

verse wavenumber,

$$\Psi_T = \frac{\lambda_{\text{lin}}''(0)}{2} \Psi_{YY} + \frac{\omega_{\text{f}}''(0)}{2} (\Psi^2)_Y, \tag{9}$$

where $\omega_f''(0)$ is given in (8) above and $\lambda_{\text{lin}}''(0) \approx 2(1 + \alpha \gamma)$ gives the effective diffusivity of transverse perturbations of the parallel striped state, obtained by perturbing the pure striped solution A_p in the y-direction with the ansatz,

$$A(\xi, y, t) = A_p(\xi, y, t; k_x, k_y) + e^{i(k_y y - \omega t)} \left[a_1 e^{\lambda t + vy} + a_2 e^{\lambda t - vy} \right],$$
(10)

collecting leading order terms in a_1, a_2 , and solving to obtain

$$\lambda = \lambda_{\text{lin}}(\mathbf{v}) = -c_g \mathbf{v} + \lambda''_{\text{lin}}(0) \mathbf{v}^2 + \mathcal{O}(\mathbf{v}^3), \ \mathbf{v} \in i\mathbb{R},$$
 (11)

where

$$c_g = \omega_f'(0) = (\alpha - \gamma)k_{x,f}'(0)(2k_{x,f}(0) - c),$$

gives the transverse group velocity for parallel stripes with $k_y = 0$. Since $k'_{x,f}(0) = 0$ one readily calculates that $c_g = \omega'_f(0) = 0$. For more details of these calculations, see Appendix A.

We remark that the modulation ansatz (10) will not be accurate in the far-field as we modulate the front uniformly in ξ . Despite this, since the interfacial dynamics will be convected into the bulk in the co-moving frame traveling with the quench, we expect our modulation to give good qualitative predictions of the far-field dynamics; see Sec. IV for brief discussion on possible extensions of our work addressing this.

1. Numerical approach

In the following examples, we give comparisons between the numerically measured transverse wavenumber dynamics of (2) and the corresponding numerical solutions of the viscous Burgers' equation (9). We simulate the quenched CGL equation using a Galerkin spectral discretization and the fast Fourier transform in both space directions on a periodic domain, $(x,y) \in [-L_x/2, L_x/2] \times [-L_y/2, L_y/2]$ with $L_x = 30\pi, L_y = 120\pi$ and $N_x = 2^8, N_y = 2^{12}$ modes in the x and y direction respectively. The quench damping level was strengthened to $\chi = -3$ for $x > L_x/4$ to surpress fluctuations coming from the periodic boundary conditions and prepare a near homogeneous state close to A=0 at the quenching line. The 4th order Runge-Kutta exponential timedifferencing algorithm of (Ref. 15) was used to time step with step sizes ranging from dt = 0.1 to dt = 0.0025; for most figures dt = 0.0025 was used. Numerical solutions of the viscous Burgers equation (9) were solved in the same manner, with spectral decomposition on the periodic computational domain $Y \in \delta[-L_v/2, L_v/2], N_v = 2^{12}$ and exponential timedifferencing in T with time-steps $\delta^2 dt$. Computations were performed in MATLAB using both CPU and GPU computations.

2. Source-sink transverse defect pair

As a case study, we study the transverse wavenumber dynamics of a defect laden solution of (2) which connects stripe solutions with small transverse wavenumber $k_{y,+} = \delta q_+$ for y > 0 and $k_{y,-} = \delta q_-$ for y > 0, with $0 < \delta \ll 1$ and $q_{\pm} = \mathscr{O}(1)$. In particular, Fig. 3 depicts a defect with $q_- = 3$ and $q_+ = 1$. Such a defect solution was obtained numerically with an initial condition of the form

$$A(\xi, y, 0) = h(-\xi) \Big(h(y) r_{-} e^{i(k_{x,-}\xi + k_{y,-}y)} + h(-y) r_{+} e^{i(k_{x,+}\xi + k_{y,+}y)} \Big),$$
(12)

where h(z) denotes the Heaviside function, $r_{\pm}^2 = \sqrt{1 - (k_{x,\pm}^2 + k_{y,\pm}^2)}$, and the wavenumbers $k_{x,\pm}$ are chosen so that $k_{x,\pm} = k_{x,\mathrm{f}}(k_{y,\pm})$, using the computed wavenumber curves depicted in Fig. 2. Since the numerical computation uses periodic boundary conditions in the vertical direction, this solution consists of two well-separated defects, one a source (left in Fig. 3b) and one a sink (right in Fig. 3b). We remark that the sink, with inward pointing group velocities in the y direction, creates a grain boundary, also known as a domain wall, in the far-field. The source, with outward pointing group velocities in the y direction, creates a wavenumber fan between the two striped states.

As the periodic wavetrains are relative equilibria, the local transverse wavenumber of the defect may be numerically measured as

$$\psi(y,t) = \text{Im}A_{y}(\xi_{0}, y, t) / A(\xi_{0}, y, t). \tag{13}$$

To determine the coefficient $\omega_f''(0)$ of the viscous Burgers equation, we measure $k_{x,f}(0)$ and $k_{x,f}''(0)$ using the numerically computed curve $k_{x,f}(k_y)$ depicted in Figure 2b. For the second-derivative, we performed a quadratic fit of the data near the origin $k_y = 0$. We then compared the measured wavenumber to the predicted transverse wavenumber dynamics coming from the Burgers' equation. We use the initial local wavenumber $\psi(y,0)$ as the initial data for the viscous Burgers' equation (9),

$$\Psi(Y,0) = \psi(Y/\delta,0)/\delta.$$

For the specific initial condition (12), $\Psi(Y,0) = q_-$ for $Y \in [-\delta L_y/2,0]$ and $\Psi(Y,0) = q_+$ for $Y \in [0,\delta L_y/2)$. We then numerically integrate forward in time the viscous Burgers' equation on the scaled periodic domain and then scale back to obtain a prediction for the transverse wavenumber dynamics at time t > 0,

$$\psi(y,t) \approx \psi_{\rm vb}(y,t) := \delta \Psi(\delta y, \delta^2 t).$$

As depicted in Figure 3, we find good agreement between the prediction from the Burgers' equation (9), which we denote as ψ_{vb} , and the numerically measured wavenumber, which we denote as $\psi_{num}(y,t)$. See Figure 4a-b for the evolution of the absolute pointwise error, which we denote as

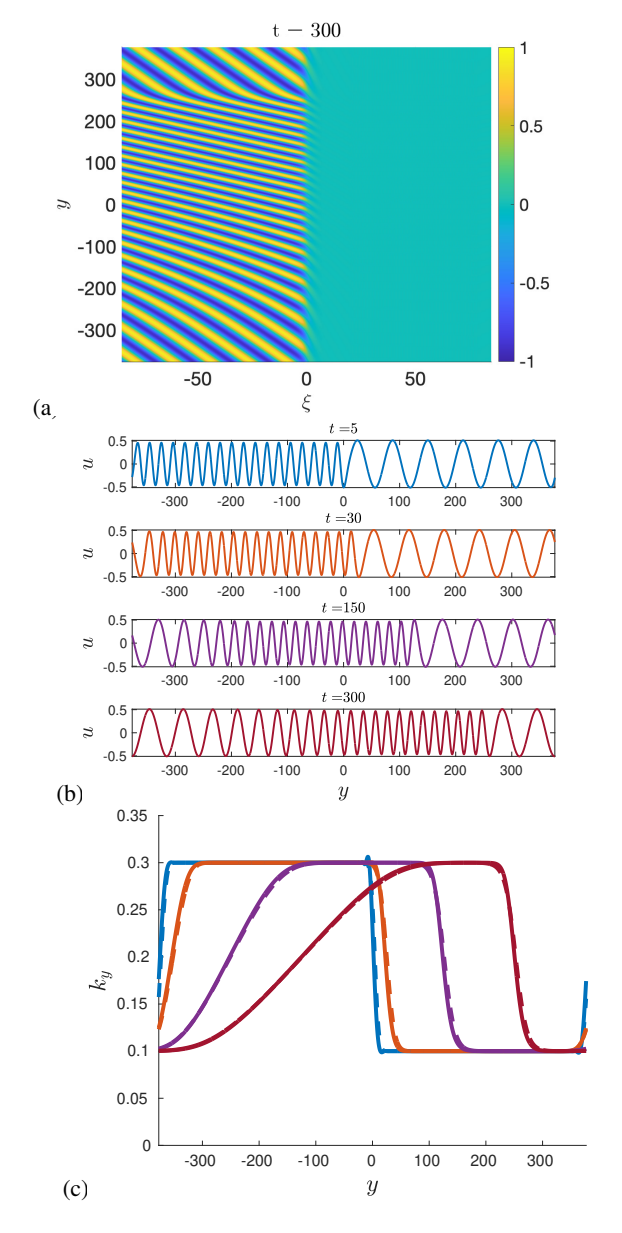


FIG. 3. Source-sink defect pair with $\alpha=3, \gamma=1, c=2.5$ obtained from initial condition (12) which connects stripes solutions with transverse wavenumbers $k_{y,-}=0.3, k_{y,+}=0.1$ and $\delta=0.1$; (a): Plot of Re $A(\xi,y,t=300)$ of (2). Note the source defect initially lies on the upper and lower domain boundaries. (b): plot of the cross-section of ReA along the line $\xi=\xi_0=-1$ for a range of times t=5(blue), 30(orange), 150(purple), 300(dark red). (c): Comparison of the local transverse wavenumber Im $\partial_y A/A$ along the line $\xi=\xi_0$ (solid), with the appropriately rescaled numerical solution of the viscous Burgers' equation (9), $\delta\Psi(\delta y, \delta^2 t)$ (dashed) with $\delta=0.1$, for same range of times. The nonlinear Burgers' parameter was calculated from data in Fig. 2b and (8) as $\omega_f''(0)=4.2126...$

 $\operatorname{Err}_{\psi}(y,t) := |\psi_{\mathrm{vb}}(y,t) - \psi_{\mathrm{num}}(y,t)|$. Figure 5 depicts errors for the wavenumber prediction for initial conditions (12) for a range of δ values. This shows that both the L^2 and L^{∞} norm of $\operatorname{Err}_{\psi}$ in y decreases as $\delta \to 0$ and the temporal regime of validity appears to scale like δ^{-2} (roughly consistent with the

results of (Ref. 14)). We also note that the initial large error and sharp decrease is due to numerical instabilities in the measured wavenumber ψ . As the wavenumber is initially discontinuous, the derivative A_y , used in the measured wavenumber (13), is calculated spectrally so that the sharp jump at $y \sim 0$ in (12) induces Gibbs-type oscillations. Parabolic regularization in (1) smooths the instantaneous jump in wavenumber, leading to a local decrease in the error for short times.

We also note that the viscous Burgers' modulation equation gives accurate predictions of the defect speed, $c_{\rm d}$, in the transverse direction. For example, considering the rightward traveling defect where $q_->q_+>0$, we use the fact that $\omega_{\rm f}''(0)>0$ to approximate the transverse group velocities, $c_{\rm g,\pm}:=\omega_{\rm f}'(k_{\rm y,\pm})\approx c_{\rm g,0}+\omega_{\rm f}''(0)\delta q_\pm$, of the asymptotic wave trains,

$$c_{g,-} > c_{d} > c_{g,+},$$
 (14)

so that they point inwards and the defect behaves as a sink. The sink defect portion of the solution in Figure 3 corresponds to a traveling shock wave solution $q_*(Y-c_*T)$ of (9) with speed c_* connecting the asymptotic states q_\pm at $Y=\pm\infty$ respectively. The Lax entropy condition for a traveling shock requires, $\omega_{\rm f}''(0)(q_--q_+)>0$. The Rankine-Hugoniot criterion in this case gives the shock speed as $c_*=(\omega_{\rm f}''(0)q_-+\omega_{\rm f}''(0)q_+)/2$. This allows us to obtain a prediction for the transverse defect speed in the full 2-D system. Since the parallel stripe has transverse group velocity $c_{g,0}:=\omega_{\rm f}'(0)=0$, we find the defect speed to be

$$c_{\rm d} = c_{\rm g,0} + \delta c_* = \delta \frac{\omega_{\rm f}''(0)}{2} (q_- + q_+).$$
 (15)

See also Sec. 1.3 of (Ref. 14) for more detail on such calculations. Figure 4c shows good agreement of the numerically measured defect speed with that predicted by the modulation equation. In particular the measured shock speed converges to the predicted speed with rate $\mathcal{O}(dt)$ as dt is reduced. We also observe that source defects with $\omega_f'(k_y^-) < c_d < \omega_f'(k_y^+)$ behave as rarefaction waves.

3. Phase-slip defect modulation

As another example, we consider a localized wavenumber perturbation of a quenched stripe in (2). Figure 6 depicts the transverse dynamics of this localized defect, initiated by an initial condition of the form

$$A(\xi, y, 0) = h(-\xi)\sqrt{1 - k^2} \exp\left[i(k_x \xi + \delta y + \phi_0(\delta y))\right],$$
(16)

where $\phi_0(Y) = \pi \operatorname{erf}(Y)$ and $\operatorname{erf}(Y) = 2\pi^{-1/2} \int_0^Y e^{-t^2} dt$ denotes the Error function. This initial condition induces a phase slip perturbation which does not alter the asymptotic wavenumber for |y| large. Here, as one moves vertically, the local phase shifts, or "slips" by half an oscillation. We refer to this defect as a phase slip (though we note that this term often refers to change of the number of zeros of the phase as

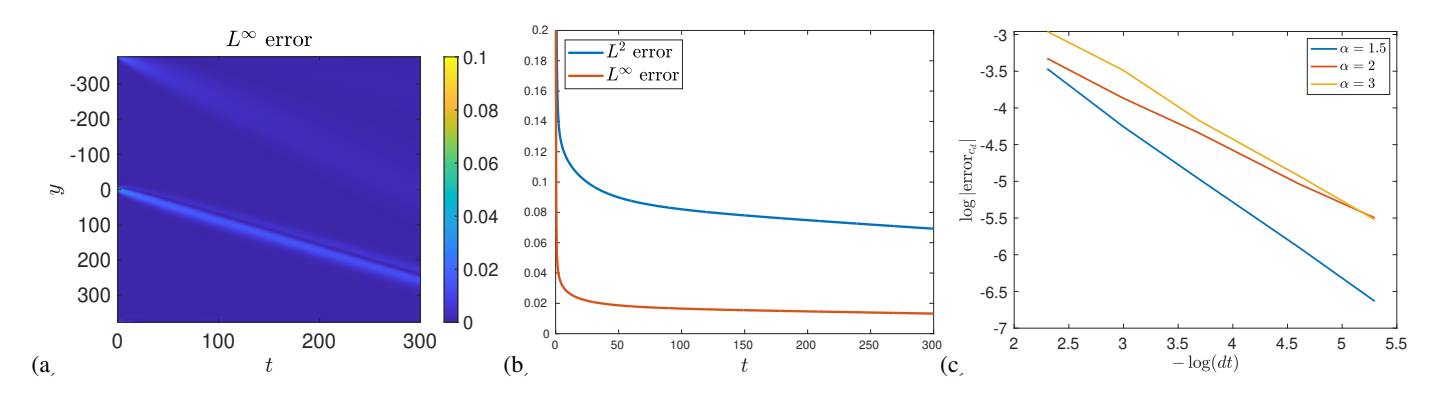


FIG. 4. (a): Spacetime diagram of the absolute error $\text{Err}_{\psi}(y,t)$ between measured transverse wavenumber $\text{Im }\partial_y A/A$ and the rescaled viscous Burgers' solution $\delta\Psi(\delta y,\delta^2 t)$, for the same initial condition and parameters as Fig. 3; (b): Plots of the corresponding L^2 and L^∞ norm of $\text{Err}_{\psi}(y,t)$ in y, note the large error for $t\sim 0$ is due to Gibbs oscillations in the measured wavenumber; (c): Plot of the dt-convergence of error between the numerically measured defect speed and the theoretical prediction $c_d=c_{g,0}+\delta c_*$, for range of α values.

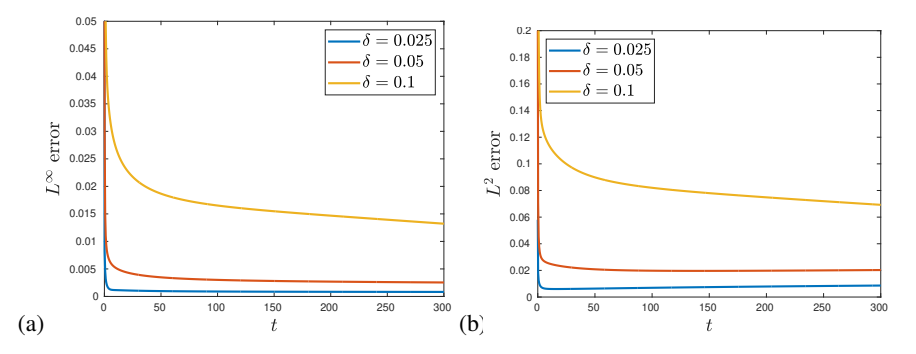


FIG. 5. Evolution of (a) the L^2 and (b) the L^∞ error, between the measured transverse wavenumber in (2) and the rescaled viscous Burgers' solution (9), for the source-sink initial data (12) for $\delta = 0.025, 0.05, 0.1$, showing decrease in the error as $\delta \to 0$. Same initial condition and parameters as Fig. 3.

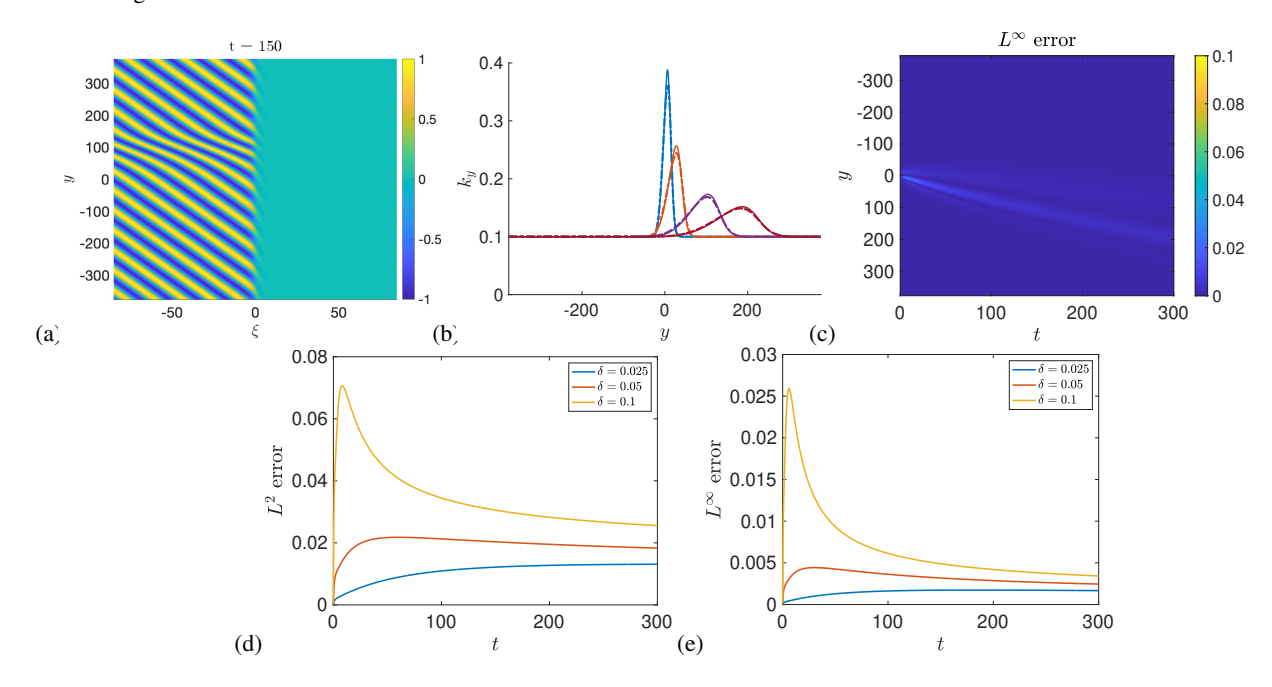


FIG. 6. Top row: Localized phase-slip defect solution of (2) with initial data (16), $c=2.5, \alpha=3, \gamma=1$ and $\delta=0.1$, numerical time step dt=0.0025. (a): plot of Re $A(\xi,y,t=150)$; (b): Comparison of numerically measured transverse wavenumber (solid line) with the associated prediction from viscous Burgers equation (9) (dashed line) for times t=5(blue), 30(orange), 150(purple), 300(dark red); (c): pointwise absolute error between measured and predicted wavenumber; Bottom row: plots of both the L^2 and L^∞ errors, (d) and (e) respectively, for the localized phase-slip for $\delta=0.025, 0.05, 0.1$.

time, not y, evolves (Ref. 16)). Such defects arise in various crystalline media, and pattern forming systems. We consider one here to highlight how they are affected by quenching mechanisms. We chose transverse wavenumber $k_y = \delta$ so that the corresponding scaled wavenumber profile satisfies $\Psi(Y) = 1 + 4\pi^{1/2} \mathrm{e}^{-Y^2}$. We once again find good agreement between the transverse wavenumber dynamics and the viscous Burgers prediction, with both L^2 and L^∞ error decreasing as δ is decreased; see Figure 6(c-e). We do note a numerical relaxation effect where the Gaussian perturbation in the Burgers' equation initially decays slightly faster than the measured wavenumber in CGL leading to slower convergence in δ compared with the source-sink initial condition (12) above.

III. MODULATIONS IN THE QUENCHED SWIFT-HOHENBERG EQUATION

To show the applicability of this approach, we also employ it to describe stripe modulations in the quenched Swift-Hohenberg (SH) equation (Ref. 17) with supercritical nonlinearity,

$$u_{t} = -(1 + \partial_{x}^{2} + \partial_{y}^{2})^{2} u + \mu \chi(x - ct) u - u^{3}, \qquad (17)$$
$$(x, y) \in \mathbb{R}^{2}, \quad \mu > 0.$$

We choose this equation as it does not have exact closed form periodic stripe solutions - only leading-order expansions at onset $0 < \mu \ll 1$ - and thus one generally must compute the viscous Burgers' coefficients, $\lambda_{\text{lin}}''(0)$ and $\omega_{\text{f}}''(0)$ with asymptotic expansions or numerically. For $\chi \equiv 1$ and $\mu > 0$, it is well-known that (17) has stable stripe equilibrium solutions $u_p(k_xx+k_yy;k)$, 2π -periodic in the first argument and dependent only on the bulk wavenumber $k^2 = k_x^2 + k_y^2$ due to the rotational invariance of the homogeneous system. The range of k values for which stripes exist and are stable is determined by the Busse balloon (Ref. 18). To study quenched fronts, we once again move into the co-moving frame $\xi = x - ct$,

$$u_{t} = -(1 + \partial_{\xi}^{2} + \partial_{y}^{2})^{2}u + c\partial_{\xi}u + \mu\chi(\xi)u - u^{3}.$$
 (18)

Previous works (Ref. 5, 8, and 19) have studied front solutions of this equation of the form $u_f(\xi, k_y y + \omega t)$, periodic in the second variable $\zeta = k_y y + \omega t$, which satisfy

$$0 = -(1 + \partial_{\xi}^{2} + k_{y}^{2} \partial_{\zeta}^{2})^{2} u_{f} + (c \partial_{\xi} - \omega \partial_{\zeta}) u_{f} + \mu \chi(\xi) u_{f} - u_{f}^{3},$$

$$(19)$$

$$0 = \lim_{\xi \to -\infty} u_{f}(\xi, \zeta), \quad 0 = \lim_{\xi \to -\infty} u_{f}(\xi, \zeta) - u_{p}(k_{x}\xi + \zeta; k),$$

$$u_{f}(\xi, \zeta) = u_{f}(\xi, \zeta + 2\pi).$$

$$(20)$$

We note that in this co-moving, co-rotating frame, under the 1:1 resonance condition $\omega = ck_x$, stripe equilibria u_p become 2π -periodic in ζ , with $k_x x + k_y y = k_x \xi + \zeta$. As in (2), the horizontal wavenumber $k_{x,f}$ of quenched front solutions, u_f , is generically selected by parameters (c,k_y) and can be written locally as a graph over these two variables. We note the works (Refs. 5 and 8) gave a near complete numerical description of

the moduli space of patterns using a far-field core numerical continuation approach. See Figure 7 for depictions of select wavenumber selection curves for c fixed and k_y varying, and vice-versa.

As before, since we shall fix c > 0, we denote these fronts as $u_f(\xi, \zeta; k_y)$, and the corresponding selected wavenumber as $k_{x,f}(k_y)$. The work (Ref. 19) showed the existence of parallel

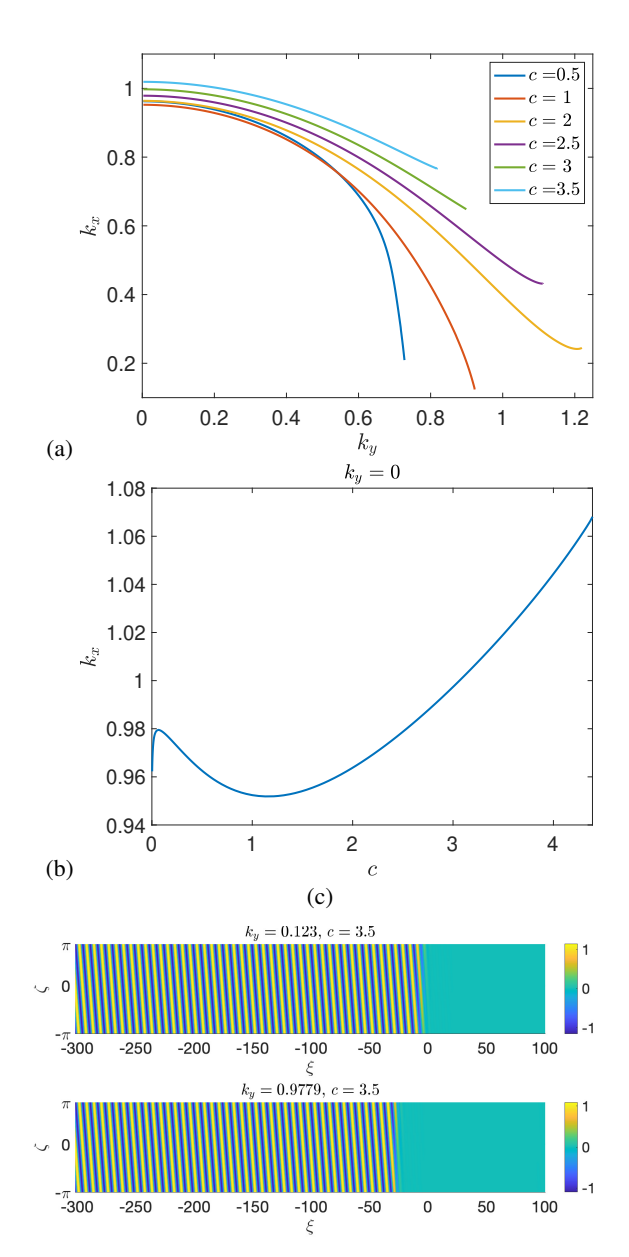


FIG. 7. Swift-Hohenberg wavenumber selection curves for $\mu=1$, depicting $k_{x,\mathrm{f}}(c,k_y)$ for (a) c fixed, and k_y varied, and (b) $k_y=0$ fixed and c varied; (c): Example front solution profiles $u_\mathrm{f}(\xi,\zeta;k_y)$ with c=3.5 and $k_y=0.123,0.9779$; $\mu=1$ throughout.

stripes with $k_y=0$ for $0<\mu\ll 1$ and in the fast quench regime where $c\lesssim c_{\rm lin}$ using center manifold techniques. It also used functional analytic techniques to prove that for any $c\in (0,c_{\rm lin})$ fixed, parallel striped fronts perturb smoothly in $k_y\sim 0$, and

the horizontal wavenumber satisfies the expansion

$$k_{x,f}(k_y) = k_{x,f}(0) + \beta_2 k_y^2 + \mathcal{O}(k_y^4),$$
 (21)

$$\beta_2 = \frac{1}{c} \langle 2\partial_{\zeta}^2 (1 + \partial_{\xi}^2) u_{\mathbf{f}}(\cdot, \cdot; 0), e_* \rangle_{L_n^2}, \qquad (22)$$

where $\langle \nu_1, \nu_2 \rangle_{L^2_\eta} = \int_{\mathbb{R} \times [0,2\pi)} \mathrm{e}^{2\eta |\xi|} \nu_1 \bar{\nu}_2 d\xi d\zeta$ denotes the exponentially-weighted L^2 inner product, and e_* spans the kernel of the L^2_η -adjoint, \mathbb{L}^* , of the linearization of (19) about the front

$$\mathbb{L}v := -\omega v_{\zeta} + cv_{\xi} - (1 + \partial_{\xi}^2)^2 v + \mu \chi v - 3(u_{\mathbf{f}}(\cdot,\cdot;0))^2 v.$$

We now briefly discuss how the parameters $\lambda''_{lin}(0)$ and $\omega''_{lin}(0)$ can be computed. The derivation of the modulation equation follows a similar line as for CGL, which is described in Appendix A.

A. Nonlinear Burgers parameter

For $\omega_f''(0)$, we use the 1:1 resonance condition and the k_y expansion (21) above to obtain

$$\omega_{f}(k_{y}) = ck_{x,f}(k_{y}) = c\left(k_{x,f}(0) + \beta_{2}k_{y}^{2} + \mathcal{O}(k_{y}^{4})\right). \tag{23}$$

This readily gives

$$\omega_{\rm f}'(0) = 0, \qquad \omega_{\rm f}''(0) = 2\beta_2 c$$
 (24)

We note that this quantity could also be obtained by differentiating the front equation twice in k_v , evaluating at $k_v = 0$

and then projecting onto the adjoint kernel element e_* defined above. In practice, we calculate $\omega_{\rm f}''(0)$ by once again performing a quadratic fit of the numerical continuation data (Fig. 7a) for the curve $k_{x,{\rm f}}(k_y)$ for $k_y\sim 0$, obtaining a numerical prediction of the quadratic coefficient β_2 . Numerical computations of these curves (see Fig. 7 as well as Refs. 8 and 20) indicate that $\omega_{\rm f}''(0)<0$ for a wide range of c values except possibly for $0< c\ll 1$.

B. Effective Diffusivity

The effective diffusivity, $\lambda_{\text{lin}}''(0)$, for y perturbations of parallel striped fronts just behind the quenching line can be obtained using a Fourier-Bloch wave analysis (Refs. 18 and 19). To summarize, one sets $k_y = 0$ and linearizes (18) about the front u_f . Since the far-field state at $\xi = +\infty$ is exponentially stable, it suffices to consider the linearization at $\xi = -\infty$, that is linearizing about the asymptotic roll state $u_p(k_x\xi + \zeta;k_x)$ with $\chi \equiv \mu$,

$$\mathbb{L}_p w := -(1+\Delta)^2 w + \mu w + c_x \partial_{\xi} w$$
$$-3u_p^2 (k_x \xi + \zeta; k_x) w - \omega \partial_{\zeta} w. \tag{25}$$

The L^2 spectrum of this operator can be studied using the Floquet-Fourier-Bloch ansatz

$$w(\xi, y, t) = e^{im\tau} e^{iny} e^{v\xi} b(k_x \xi + \zeta; m, n, v),$$

$$m \in \mathbb{Z}, n \in \mathbb{R}, v \in i[0, 2\pi/k_x).$$
(26)

for b(z; m, n, v) a 2π -periodic function in z. Inserting this into $\mathbb{L}_p w = \lambda w$, and using the fact that $\omega = ck_x$, we obtain a family of eigenvalue problems

$$\lambda b = \mathcal{B}(m, n, v)b := -(1 + (k_x \partial_z + v)^2 - n^2)^2 b + \mu b + (c_x v - \omega i m)b - 3u_p(z; k_x)^2 b. \tag{27}$$

Evaluating (27) at m=0, n=0, v=0, we find that $b=\partial_z u_p$ is an eigenfunction with eigenvalue $\lambda=0$. A perturbative approach then gives a family of eigenvalue-eigenfunction pairs $(\lambda_{\text{lin}}(v), w_{\text{lin}}(v))$ emanating from $(0, \partial_z u_p)$. Since $\mathcal{B}(0, 0, 0)$ is $L^2([0, 2\pi))$ -self-adjoint with $\ker \mathcal{B}(0, 0, 0) = \operatorname{span} \partial_z u_p$, we also have that $\partial_z u_p \in \operatorname{Rg} \mathcal{B}(0, 0, 0)^{\perp}$. Letting b_* be a scalar multiple of $\partial_z u_p$ so that $\langle b_*, b_* \rangle_{L^2(0, 2\pi)} = 1$, and differentiating the eigenvalue equation (27) in v, we obtain

$$\lambda_{\text{lin}}''(0) = \langle 4(1 + (k_x \partial_z)^2) \partial_z u_p, b_* \rangle_{L^2(\mathbb{T}_{2\pi})}.$$
 (28)

To obtain a numerical discretization of the kernel element b_* , we computed this inner product numerically using Newton's method to solve a finite difference discretization of the periodic boundary value problem $0 = -(1 + k^2 \partial_{\theta}^2)^2 u_p + \mu u_p - u^2$, and an iterative linear solver.

C. Slowly-varying transverse modulations

We are now able to provide a modulational description of transverse wavenumber dynamics in (18). We shall once again focus on parallel striped fronts. Fix a c>0 where parallel striped fronts $u_{\rm f}(\xi,\omega t;k_x)$ exist, and are diffusively stable. Fixing $\xi=\xi_0<0$ just behind the quenching line, we consider a modulation of the traveling front solution through the ansatz, $u_{\rm f}(\xi,\Phi(Y,T)+\omega t;\delta\Phi_Y(Y,T))+\delta^2w_1(\xi,Y,T;\delta)$. Inserting and expanding in δ , we once again obtain a viscous Burgers' modulation equation (9) for the transverse wavenumber Ψ with the coefficients $\lambda''_{\rm lin}(0)$ and $\omega''_{\rm f}(0)$ found above. In all numerical simulations of (9) discussed below, we use the numerical approximations of these coefficients as described above.

Using this modulation equation, we obtain accurate predictions for the transverse wavenumber evolution. In Figure 8 we consider a localized phase perturbation of a weakly oblique stripe of the same form as in (16). To measure the transverse

wavenumber we use the Hilbert transform

$$\mathcal{H}[u](y) := \mathcal{F}^{-1}\left[-i\operatorname{sign}(\ell)\mathcal{F}[u](\ell)\right](y),$$

where $\mathscr{F}[u](\ell)$ denotes the Fourier transform in y and ℓ the Fourier wavenumber variable, to construct a complex signal $v(y) = u(y) + i\mathscr{H}[u](y)$. For oscillatory functions $u(y) \approx \cos(\phi(y))$, this can be differentiated to obtain a local wavenumber $\psi(y,t) = \operatorname{Im} \partial_y v/v$. As the Hilbert transform induces spurious oscillations in the measured wavenumber, we use the iterative transform approach of (Ref. 21) to reduce, though not eliminate, the occurrence and magnitude of such oscillations. We found 15-20 iterations of this approach gave sufficient convergence, with little no significant improvement for more iterations. Once again using a scaled version of the initial wavenumber, $\delta^{-1}\psi(Y/\delta,0)$, as the initial data for the Burgers' equation (9), we find good agreement between the predicted and measured wavenumbers, with errors behaving similarly as those in CGL.

In Figure 9 we consider a pair of symmetric grain boundary defects which connect weakly oblique stripes of the opposite wavenumber $k_v = \pm \delta$, with one grain boundary convex to the quench line and the other concave. This solution was initialized with initial data similar to (12) with discontinous transverse wavenumber. The convex grain, located in the middle of the computational domain, has left wavenumber $k_{v,-} = -\delta$ and right wavenumber $k_{y,+} = +\delta$. Since, $\omega_f''(0) < 0$, this defect behaves as a shock-like sink in the transverse direction, with speed $c_* = \boldsymbol{\omega}''(0)(k_{\nu,-} + k_{\nu,-})/2 = 0$ and wavenumber interface which remains sharply localized. The concave grain, located near the boundary of the periodic computational domain, has "left" wavenumber $k_{v,-} = \delta$ and "right" wavenumber $k_{y,+} = -\delta$. Thus the corresponding solution to the Burgers' equation has outward pointing characteristics and thus behaves like a rarefaction wave.

We remark here that wavenumber measurements using the Hilbert transform (which in MATLAB uses the discrete Fourier transform) induce Gibbs-type oscillations due to the sharp viscous shock profile in the wavenumber, leading to larger errors in the part of the domain where the shock resides. We remark that we also studied an asymmetric grain boundary in (18) with moving shock and rarefaction wave as studied in CGL and depicted in Figure 3 above. While not depicted, we obtained accurate shock speed predictions from the viscous Burgers modulational approximation.

IV. CONCLUSION AND DISCUSSION

To summarize, we derived a one-dimensional viscous Burgers' modulation equation to describe small-amplitude transverse wavenumber dynamics of asymptotically-stable striped patterns in the wake of a rigidly propagating directional quench. Of most interest, we found that the nonlinear flux coefficient, $\omega_f''(0)$, is determined through the wavenumber selection properties of the directional quench. Somewhat less surprisingly, the viscosity coefficient, $\lambda_{\text{lin}}''(0)$, in the modulation equation is determined by the transverse diffusivity

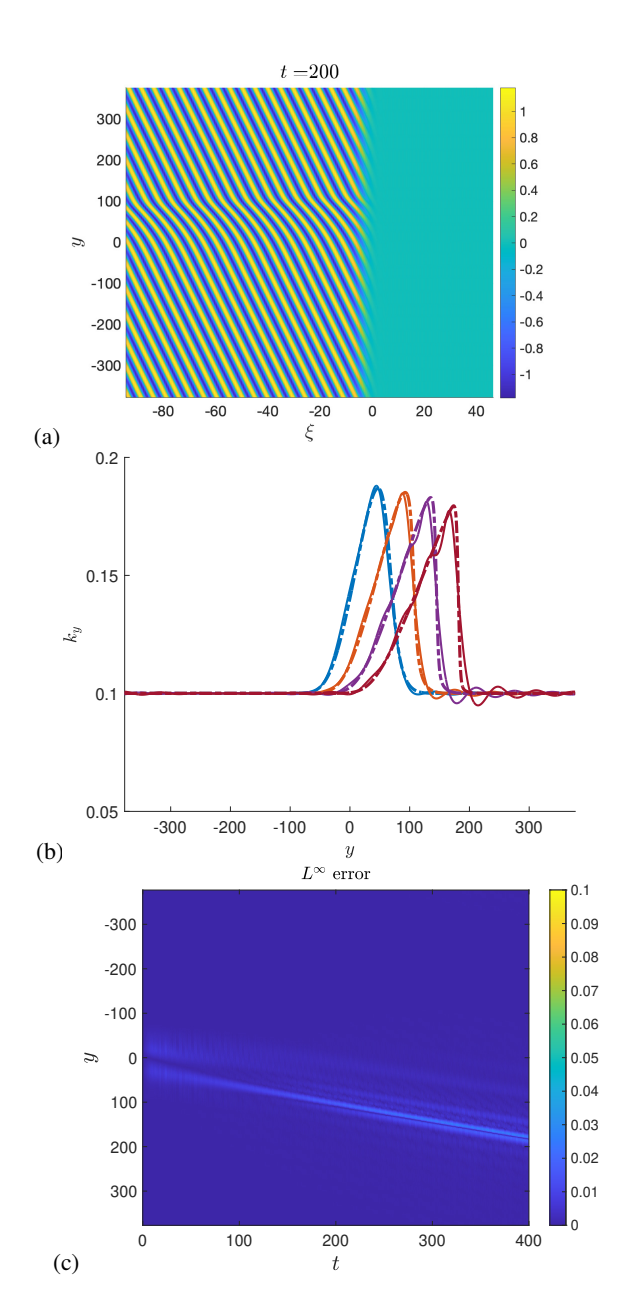


FIG. 8. Localized phase perturbation in equation (18) of a striped front with $(k_x, k_y) = (0.993, 0.1)$; Initial condition $u(\xi, y, 0) = \sqrt{4\mu/3}\cos(k_xx + k_yy + \phi_0(\delta y))h(-\xi)$ (similar to (16)), with $c = 3, \mu = 1$; the Burger's parameters were computed numerically as $\lambda''_{lin}(0) = 0.3202...$, $\omega''_{l}(0) = -2.67471...$; (a): solution profile $u(\xi, y, t = 200)$, (b): Transverse wavenumber dynamics at $\xi = \xi_0 = -1$ fixed (solid) plotted against the rescaled viscous Burgers' solution (9) at times t = 100(blue), 200(orange), 300(purple), 400(red); (c): plot of absolute error between measured and predicted wavenumber profiles.

of pure stripes. This modulation equation accurately predicted finite-time dynamics of small amplitude wavenumber defects just behind the quenching line, including source-sink pairs and localized phase-slip defects, in both the complex Ginzburg-Landau and Swift-Hohenberg equations. While we only considered examples of coherent defects, we expect the

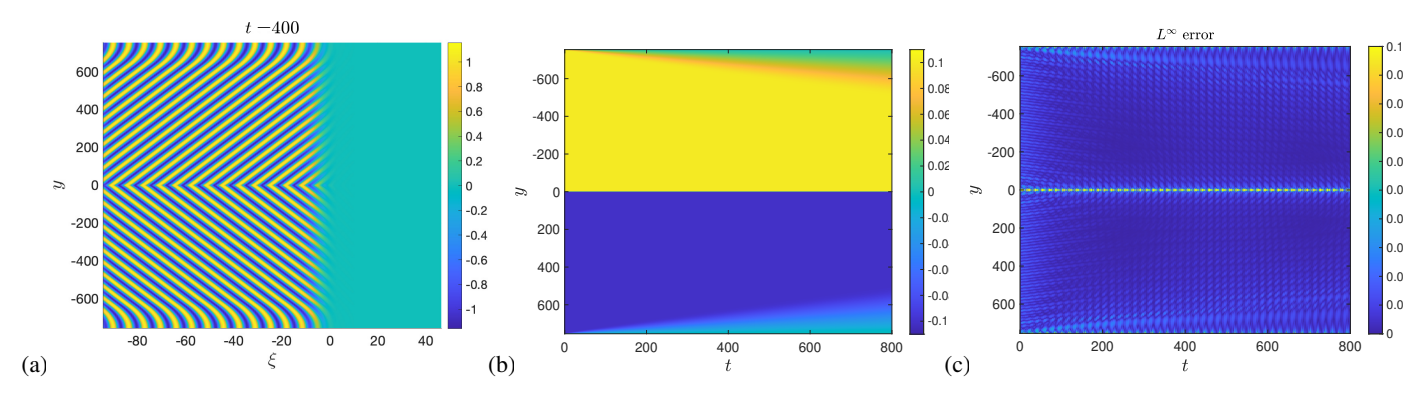


FIG. 9. Grain boundary defect in equation (18) with $c = 3, \mu = 1$, and Burger's parameters as in Fig. 8; (a): snapshot of grain boundary type solution of (18) with $\mu = 1, c = 3$, and transverse wavenumbers $k_y = \pm 0.1$, plotted at t = 400, with convex grain boundary at center of domain $y \sim 0$, and concave grain boundary at the boundary of the (periodic) computational domain. Center: space-time diagram of corresponding rescaled Burgers' solution $\delta \Psi(\delta y, \delta^2 t)$ of (9); Right: spacetime diagram of absolute error between measured and predicted wavenumbers.

modulation equation to give accurate predictions for arbitrary wavenumber modulations which are smooth and smallamplitude. Furthermore, we expect this modulational analysis to accurately predict the dynamics of directionally quenched stripes in general dissipative systems where the underlying asymptotic pattern is diffusively stable and the quench selects wavenumbers. That is, for a fixed quenched speed c and transverse wavenumber k_v , the horizontal wavenumber k_r is locally unique. A few examples include reaction-diffusion systems such as the CDIMA system mentioned above (Ref. 4), biologically motivated systems arising in morphogenesis, tissue, and digit patterning (see Ref. 22 and references therein), and ramped convection rolls (Ref. 1). It would also be interesting to investigate the suitability of this analysis to quenched patterns in phase separative systems where mass conservation can play a role (see for example Ref. 23–26).

There are several areas of further study to extend from this work. The first and most natural next step would be to consider the far-field dynamics by deriving a two-dimensional modulational equation for the striped phase or wavenumber in the half-plane to the left of the quenching line at x = ct, with vertical boundary condition along the *y*-axis. One would seek to derive a Hamilton-Jacobi equation (Ref. 27) or Cross-Newell phase diffusion equation (Refs. 28 and 29) for the phase dynamics, possibly through an intermediate Newell-Whitehead-Segel amplitude equation (Ref. 30). Of most interest would be to determine a suitable boundary condition for the phase to represent the quenching line.

In the limit of slow quenching speed, the work (Ref. 31) used a linear phase-diffusion equation $\varphi_t = \Delta \varphi + c \varphi_x$, with nonlinear boundary condition $\varphi_x = g(\varphi)$, $(x,y) \in \{0\} \times \mathbb{R}$ on the vertical axis, to describe the dynamics of the phase φ . Here the nonlinear boundary condition is determined by an object known as the *strain-displacement* relation of stationary quenched stripes, a curve which parameterizes the set of possible wavenumbers selected by the quench in terms of the asymptotic phase. For the phase dynamics observed above, a linear equation of this form will not accurately represent shock dynamics in the far-field where gradients may become sharp. Moreover, we do not expect such a model to be valid for inter-

mediate or fast growth where phases are rapidly shed from the quenching line and are also dependent on the local transverse wavenumber. To our knowledge, an appropriate boundary condition has not been derived for these regimes. Such a phase description would allow one to understand the precise far-field behavior of the defects observed above. For example, they would allow one to describe how the Swift-Hohenberg grain-boundary formed in Figure 9 relaxes or evolves as $x \to -\infty$.

Furthermore, in the context of the CGL equation, one could derive a nonlinear anisotropic phase diffusion equation by slowly modulating a pure horizontal stripe of wavenumber $k_{x,\mathrm{f}}(0)$ in (2) in both the ξ and y directions. In particular, one could restrict to $x \leq 0$ so that $\chi \equiv 1$ and modulate the selected horizontal striped phase (instead of the front A_{tf}) with an ansatz of the form,

$$A = A_{ph} = (r + \delta R) \exp \left[i \left(k_{x,f}(0) \xi - \omega t + \varphi(X, Y, T) \right) \right], \tag{29}$$

with $(X,Y,T) = \delta(\xi,y,\delta t)$. This yields,

$$\varphi_T = (1 + \alpha \gamma) \Delta_{X,Y} \varphi + D_{||} \varphi_{XX} + + (2k_{x,f}(0)(\gamma - \alpha) + c) \varphi_X + (\gamma - \alpha) |\nabla_{X,Y} \varphi|^2$$
(30)

with
$$D_{||} = -\frac{2k_{x,f}(0)^2(1+\gamma^2)}{1-k_{x,f}(0)^2}$$
; see for example (Ref. 32–36).

To represent the effect of the quench in this 2D phase equation, we propose a phenomenological nonlinear boundary condition at X=0 which uses the selected wavenumber function, $k_{x,f}$, to connect the local horizontal and vertical wavenumbers, $\delta \varphi_X$ and $\delta \varphi_Y$ respectively,

$$\delta \varphi_X = k_{x,f}(\delta \varphi_Y) - k_{x,f}(0), \qquad X = 0.$$
 (31)

For $0 < \delta \ll 1$, we can then use the expansion of $k_{x,f}$ to reduce to the quadratic approximation

$$\varphi_X = \frac{k_{x,f}''(0)}{2} \delta(\varphi_Y)^2, \qquad X = 0.$$
(32)

Figure 10 provides the results of a preliminary numerical simulation of (30) on the domain $(X,Y) \in \delta[-L_x/2,0] \times$

 $\delta[-L_y/2, L_y/2]$. The quadratic approximation (32) of the nonlinear boundary condition was used on the right boundary at X=0, a Neumann boundary condition, $\Phi_X=0$, on the left boundary at $X=-\delta L_x/2$, and shifted periodic boundary conditions

$$\varphi(X, -\delta L_{\nu}/2) = \varphi(X, \delta L_{\nu}/2) + 2\pi m, \tag{33}$$

on the top and bottom boundaries. This condition allows the phase φ to wind across the vertical domain, where m is some integer chosen to fit the given initial condition. This simulation uses the scaled phase-slip defect of (16), $\varphi(X,Y,0) = 1 +$ $\pi \operatorname{erf}(Y)$. In order to implement the nonlinear boundary condition on the right-side, centered 2nd-order finite differences were used in space with $N_x = 2^7$ and $N_y = 2^{10}$ grid points. Implicit-explicit Crank-Nicolson time-stepping was used with $dT = \delta^2 dt$. Note the plotted solutions are scaled back onto the CGL domain $(\xi, y) = (X, Y)/\delta$. Figure 10 compares $A(\xi, y, t)$ against the predicted modulated phase $\delta \varphi(\delta \xi, \delta y, \delta^2 t)$. Figure 10(b) gives the reconstructed phase A_{ph} from (29) using the modulated phase $\delta \varphi$, while 10(c) and (d) give the rescaled wavenumber perturbations $\delta \varphi_X$ and $\delta \varphi_Y$ respectively. We point out how the transverse defect starting at Y = 0 induces, through the nonlinear boundary condition at X = 0, a horizontal wavenumber perturbation which then convects and spreads vertically and leftward. As the proposed nonlinear boundary condition is only heuristic, we leave more quantitative analysis and comparison to future work.

We also mention that one can heuristically obtain the transverse modulation equation (9) used throughout this work by adding $(k_{x,f}''(0)/2)k_y^2$ to the phase φ in (30), substituting $k_y \sim \varphi_Y$ and restricting only to Y-dependent terms. After obtaining such a two-dimensional approximation, it would also be of interest to obtain rigorous approximation results, as given in (Ref. 14), between the modulation equation and the full system.

Other avenues of subsequent study include extending this analysis to three spatial dimensions $(x, y, z) \in \mathbb{R}^3$ with a planar quench propagating in the *x*-direction and a modulation equation for the two-dimensional transverse dynamics in (y, z). Finally, it would be of interest to derive transverse modulation equations for non-directional quenching where the interface bounding the pattern-forming regime is not a hyperplane, but an evolving curve or sub-manifold.

ACKNOWLEDGMENTS

The authors were partially supported by the National Science Foundation through grants NSF-DMS-2006887 and DMS-2307650.

DATA AVAILABILITY STATEMENT

The data and code that support the findings of this study are available from the corresponding author upon reasonable request.

AUTHOR CONTRIBUTIONS

Sierra Dunn: writing – review and editing (equal); numerical computations (equal); formal analysis (supporting). **Ryan Goh**: Conceptualization (lead); writing – original draft (lead); writing – review and editing (equal); formal analysis (lead); numerical computations (equal). **Benjamin Krewson**: writing – review and editing (equal); numerical computations (equal); formal analysis (supporting).

Appendix A: Derivation of transverse modulation equation

Below we provide the derivation of the transverse modulation equation (9) for the quenched CGL equation (2). An analogous approach gives the same modulation equation for the quenched SH equation (18).

We seek to modulate the traveling wave solutions $A_*(\xi, y, t; k_y) := e^{i(k_y y - \omega t)} A_f(\xi; k_y)$ of (2) described above, where A_f is a solution of the traveling wave equation (5). We write the latter equation in the condensed form

$$0 = L(k_{y})A + N(A,\bar{A}),$$

$$L(k_{y}) = (1 + i\alpha)(\partial_{\xi}^{2} - k_{y}^{2}) + c\partial_{\xi} + \chi - i\omega_{f}(k_{y}),$$

$$N(A,\bar{A}) = -(1 + i\gamma)A^{2}\bar{A} = -(1 + i\gamma)A|A|^{2},$$
(A1)

where we recall that $\omega_f(k_y)$ is the selected frequency of the quenched front determined by k_y .

Note, to obtain a smooth equation, we consider A and \bar{A} independently, and hence must also consider the complex conjugate of (A1). Taken together, denoting $U = (A, \bar{A})^T$, we thus consider

$$\begin{pmatrix} 0 \\ 0 \end{pmatrix} = \mathscr{F}(U; k_y) := \mathscr{L}(k_y)U + \mathscr{N}(U), \tag{A2}$$

$$\mathscr{L}(k_{y}) := \begin{pmatrix} L(k_{y}) & 0\\ 0 & \bar{L}(k_{y}) \end{pmatrix}, \ \mathscr{N} = \begin{pmatrix} N(U)\\ \bar{N}(U) \end{pmatrix}. \tag{A3}$$

1. Transverse wavenumber dependence and stability of CGL front

Before performing the modulation expansion, we consider some properties of (A2), its dependence on k_y , and its linearization. To begin, we evaluate the equation on the front, $0 = \mathcal{F}(U_f(\cdot; k_y); k_y)$ and differentiate in k_y to first and second order, obtaining

$$0 = [\mathcal{L}(k_y) + D\mathcal{N}(U_f)] \partial_{k_y} U_f(k_y) + \partial_{k_y} \mathcal{L}(k_y) U_f(k_y), \quad (A4)$$

$$0 = [\mathcal{L}(k_y) + D\mathcal{N}(U_f)] \partial_{k_y}^2 U_f(k_y) + 2\partial_{k_y} \mathcal{L}(k_y) \partial_{k_y} U_f(k_y)$$

$$+ D^2 \mathcal{N}(U_f) [\partial_{k_y} U_f(k_y), \partial_{k_y} U_f(k_y)]. \quad (A5)$$

with Jacobian

$$D\mathcal{N}\left(\frac{A}{\bar{A}}\right) = -\left(\begin{array}{cc} 2(1+\mathrm{i}\gamma)A\bar{A} & (1+\mathrm{i}\gamma)A^2\\ (1-\mathrm{i}\gamma)\bar{A}^2 & 2(1-\mathrm{i}\gamma)A\bar{A} \end{array}\right),$$

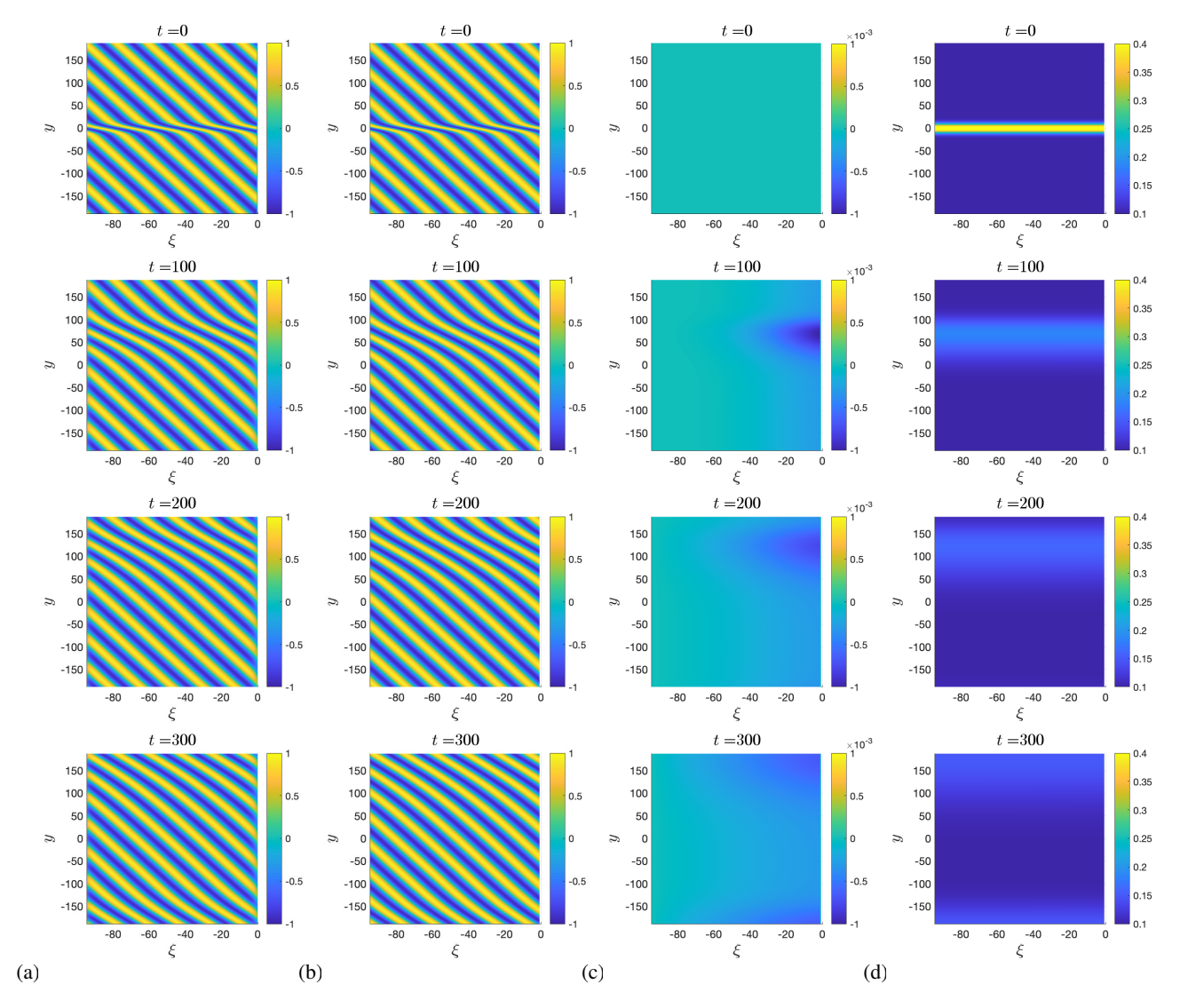


FIG. 10. (a): Solution of (2) with initial data (16), c = 2.5, $\alpha = 3$, $\gamma = 1$ and $\delta = 0.1$, numerical time step dt = 0.0025 with $N_x = 2^8$, $N_y = 2^{10}$, $L_x = 30\pi$, $L_y = 60\pi$, and other numerical details as in Sec. II B 1; (b): Reconstructed signal $A_{\rm ph}$ defined in (29) using the rescaled solution $\varphi(\delta\xi, \delta y, \delta^2 t)$ of the phase diffusion equation (30); (c): horizontal derivative of rescaled solution $\delta\varphi_X(\delta\xi, \delta y, \delta^2 t)$ of (30); (d): vertical derivative of rescaled solution $\delta\varphi_Y(\delta\xi, \delta y, \delta^2 t)$ of (30);

and vector-valued quadratic term

$$D^{2}\mathcal{N}(U_{f})[U,V] := \left(D^{2}N(U_{f})[U,V], D^{2}\bar{N}(U_{f})[U,V]\right)^{T}$$

with Hessian quadratic forms

$$\begin{split} D^2 N(U_{\rm f}) \left[U, V \right] &= -2 (1+\mathrm{i}\gamma) U^T \left(\begin{array}{cc} \bar{A}_{\rm f} & A_{\rm f} \\ A_{\rm f} & 0 \end{array} \right) V \\ D^2 \bar{N}(U_{\rm f}) \left[U, V \right] &= -2 (1-\mathrm{i}\gamma) U^T \left(\begin{array}{cc} 0 & \bar{A}_{\rm f} \\ \bar{A}_{\rm f} & A_{\rm f} \end{array} \right) V. \end{split}$$

Evaluating at $k_y=0$ and recalling from (7) above that $\partial_{k_y}\omega(0)=0$, we have that $\partial_{k_y}\mathscr{L}(0)=0$ and

Next, the gauge action $(A,\bar{A}) \mapsto (\mathrm{e}^{\mathrm{i}\theta}A,\mathrm{e}^{-\mathrm{i}\theta}\bar{A})$, induces a 0-eigenvalue with eigenfunction $U_0 := (\mathrm{i}A_\mathrm{f},-\mathrm{i}A_\mathrm{f})^T$ of the linearization

$$\mathbb{L} := \mathscr{L}(0) + D\mathscr{N}(U_{\mathbf{f}}(0))$$

of \mathscr{F} at $(U,k_y)=(U_{\mathrm{f}}(\cdot;0),0)$, defined in an exponentially weighted function space with growing weights at $\xi=\pm\infty$. Due to the lack of ξ -translational invariance caused by the inhomogeneous quenching term, we find $\ker \mathbb{L}=\mathrm{span}\{U_0\}$. One also can define the formal adjoint of \mathbb{L} as

$$\mathbb{L}^{\mathrm{ad}} := \left(\begin{array}{cc} L(0)^{\mathrm{ad}} & 0 \\ 0 & L(0)^{\mathrm{ad}} \end{array} \right) + D\mathscr{N}(U_{\mathrm{f}})^*,$$

$$\partial_{k_y}^2 \mathscr{L}(0) = \left(\begin{array}{cc} -2(1+\mathrm{i}\alpha) & 0 \\ 0 & -2(1-\mathrm{i}\alpha) \end{array} \right) + \partial_{k_y}^2 \omega_\mathrm{f}(0) \left(\begin{array}{cc} -\mathrm{i} & 0 \\ 0 & \mathrm{i} \end{array} \right) \\ \text{where } L(0)^\mathrm{ad} = (1-\mathrm{i}\alpha)\partial_\xi^2 - c\partial_\xi + \chi - \mathrm{i}\omega_\mathrm{f} \text{ and } * \text{ denotes and } * \mathrm{denotes } + \mathrm{i}\omega_\mathrm{f} \\ \mathrm{denotes } + \mathrm{i}\omega_\mathrm{f} + \mathrm{i}\omega_\mathrm{f} + \mathrm{i}\omega_\mathrm{f} \\ \mathrm{denotes } + \mathrm{i}\omega_\mathrm{f} + \mathrm{i}\omega_\mathrm{f} \\ \mathrm{denotes } + \mathrm{i}\omega_\mathrm{f} + \mathrm{i}\omega_\mathrm{f} + \mathrm{i}\omega_\mathrm{f} \\ \mathrm{denotes } + \mathrm{i}\omega_\mathrm{f} + \mathrm{i}\omega_\mathrm{f} + \mathrm{i}\omega_\mathrm{f} + \mathrm{i}\omega_\mathrm{f} \\ \mathrm{denotes } + \mathrm{i}\omega_\mathrm{f} \\ \mathrm{denotes } + \mathrm{i}\omega_\mathrm{f} + \mathrm{i}\omega_\mathrm{f$$

let U^{ad} denote the element spanning $\ker \mathbb{L}^*$ which satisfies $\langle U^{\mathrm{ad}}, U_0 \rangle_{L^2(\mathbb{R})^2} = 1$.

Evaluating (A4) at $k_y = 0$ we find that $\partial_{k_y} U_f$, if it is non-trivial, must lie in ker \mathbb{L} . Evaluating (A5) at $k_y = 0$ and moving the term involving $\partial_{k_y}^2 \mathcal{L}(0)$ over to one side, we obtain

$$\begin{split} \partial_{k_{y}}^{2} \mathscr{L}(0) U_{\mathrm{f}} &= - \left[\left(\mathscr{L}(0) + D \mathscr{N}(U_{\mathrm{f}}) \right) \partial_{k_{y}}^{2} U_{\mathrm{f}} \right. \\ &\left. + D^{2} \mathscr{N}(U_{\mathrm{f}}) [\partial_{k_{y}} U_{\mathrm{f}}, \partial_{k_{y}} U_{\mathrm{f}}] \right]. \end{split} \tag{A6}$$

Taking the $L^2(\mathbb{R})$ inner product with U^{ad} , we then obtain

$$\begin{split} &-\partial_{k_{y}}^{2}\omega_{f}(0) = \left\langle U^{ad}, -\partial_{k_{y}}^{2}\omega(0)U_{0}\right\rangle \\ &= 2\left\langle U^{ad}, \left(\begin{array}{c} (1+i\alpha)A_{f} \\ (1-i\alpha)\bar{A}_{f} \end{array} \right) \right\rangle - \left\langle U^{ad}, D^{2}\mathcal{N}(U_{f})[\partial_{k_{y}}U_{f}, \partial_{k_{y}}U_{f}] \right\rangle. \end{split} \tag{A7}$$

In principle, one could numerically approximate the inner products on the right hand side. As described in the main body of the text, we numerically continue front-wavenumber pairs $(A_f, k_{x,f})$ in k_y . This allows us to estimate derivatives of the curve $k_{x,f}$ and thus compute $\omega_f''(0)$.

To obtain the viscosity parameter of the modulation equation, we also need to consider the linearized dynamics of transverse perturbations of the parallel-striped front near the interface. To begin, we consider transversely modulated perturbations of the parallel striped front $A = e^{i\omega t} \left(A_f(\xi;0) + a(\xi,t)e^{vy}\right), \ v \in i\mathbb{R}$ in equation (2), and obtain at the linear level in a and \bar{a} , after including the complex conjugate equation, the system

$$V_t = \widetilde{\mathbb{L}}(v)V, \tag{A8}$$

$$V = (a, \bar{a})^T, \quad \widetilde{\mathbb{L}}(v) = \begin{pmatrix} \tilde{L}(v) & 0 \\ 0 & \overline{\tilde{L}}(v) \end{pmatrix} + D\mathcal{N}(U_f),$$

where $\tilde{L}(v) = (1+i\alpha)(\partial_{\xi}^2 + v^2) + c\partial_{\xi} + \chi - i\omega_{\rm f}(0)$ (compare to the operator $L(k_y)$ in (A1)). We then consider transversely modulated eigenvalues

$$\widetilde{\mathbb{L}}(\mathbf{v})V(\mathbf{v}) = \lambda_{\text{lin}}(\mathbf{v})V(\mathbf{v}),$$

where $V(0) = U_0$ gives the gauge-action eigenfunction with eigenvalue $\lambda_{\text{lin}}(0) = 0$ discussed above. In a similar manner to the k_y dependence of the front in Section A 1, we twice-differentiate the eigenvalue equation with respect to ν , evaluate at $\nu = 0$, use the fact that $\partial_{\nu} \tilde{\mathbb{L}}(0) = 0$, and take the inner product with U_{ad} to obtain

$$\lambda_{\text{lin}}''(0) = 2 \left\langle \left(\begin{array}{c} i(1+i\alpha)A_0 \\ -i(1-i\alpha)A_0 \end{array} \right), U_{\text{ad}} \right\rangle. \tag{A9}$$

We approximate $\lambda_{\text{lin}}''(0)$ by considering transverse perturbations of a pure parallel-stripe. Following (Ref. 10), we perturb stripes with the ansatz $A(x,y,t) = \mathrm{e}^{\mathrm{i}\omega t} \left[r_{\mathrm{f}} \mathrm{e}^{\mathrm{i}k_{\mathrm{f}}x} + a_{+} \mathrm{e}^{\lambda t + vy} + a_{-} \mathrm{e}^{\bar{\lambda}t - vy} \right]$ in (2), collecting $\mathscr{O}(a_{\pm})$ terms, solving for λ , and expanding in $v \sim 0$ to obtain

$$\lambda_{\text{lin}}(v) = (1 + \alpha \gamma)v^2 - \frac{\alpha^2}{2}(1 + \gamma^2)v^4 + \mathcal{O}(v^6), \quad v \in i\mathbb{R}.$$
(A10)

Importantly, our assumption that the selected asymptotic waves are Benjamin-Feir stable, $1 + \alpha \gamma > 0$, gives $\lambda_{\text{lin}}''(0) > 0$.

2. Modulational ansatz and expansion

As described above, we consider the modulational ansatz

$$A(\xi, y, t) = e^{i(\Phi - \omega t)} \left(A_f(x; \delta \Phi_Y) + \delta^2 w_1(\xi, Y, T; \delta) \right),$$

with $\Phi = \Phi(Y, T)$ a long-wavenlength phase modulation function of the variables $Y = \delta y$ and $T = \delta^2 t$ and a higher order correction term w_1 , for $0 < \delta \ll 1$. We then expand

$$\begin{split} A_{\mathrm{f}}(\xi;\delta\Phi_{Y}) = & A_{\mathrm{f}}(\xi;0) + \delta\Phi_{Y}\partial_{k_{y}}A_{\mathrm{f}}(\xi;0) \\ & + \frac{\delta^{2}}{2}\Phi_{Y}^{2}\partial_{k_{y}}^{2}A_{\mathrm{f}}(\xi;0) + \mathscr{O}(\delta^{3}). \end{split}$$

Note, to ease notational burden, we let $A_0 = A_f, A_1 = \partial_{k_y} A_f$, $A_2 = \partial_{k_y}^2 A_f$, and we also set $U_j = (A_j, \bar{A}_j)^T$ for j = 1, 2. Before inserting this expansion into (2), we calculate several derivatives of the expanded ansatz $e^{i(\Phi - \omega t)}(A_f(\xi; \delta \Phi_Y) + \delta^2 w_1)$:

$$\begin{split} \partial_t A(\xi,y,t) &= -\mathrm{i} \omega A_0 - \delta \mathrm{i} \omega \Phi_Y A_1 \\ &+ \delta^2 \left(\mathrm{i} \Phi_T A_0 - \mathrm{i} \omega \left(\frac{\Phi_Y^2}{2} A_2 + w_1 \right) \right) + \mathscr{O}(\delta^3), \\ \partial_y^2 A(\xi,y,t) &= \delta^2 \left(\mathrm{i} \Phi_{YY} A_0 - \Phi_Y^2 A_0 \right) + \mathscr{O}(\delta^3). \end{split}$$

The cubic nonlinearity expands as

$$\begin{split} A^2 \bar{A} &= A_0^2 \bar{A}_0 + \delta \left(2A_0 \bar{A}_0 A_1 \Phi_Y + A_0^2 \bar{A}_1 \Phi_Y \right) \\ &+ \delta^2 \left(A_0 \bar{A}_0 (A_2 \Phi_Y^2 + 2w_1) + A_0^2 (\bar{A}_2 \frac{\Phi_Y^2}{2} + w_1) \right. \\ &+ \bar{A}_0 A_1^2 \Phi_Y^2 + 2A_0 \Phi_Y^2 A_1 \bar{A}_1 \right) + \mathscr{O}(\delta^3), \end{split} \tag{A11}$$

while the expansion for $A\bar{A}^2$ is obtained by taking complex conjugates. Inserting the expanded ansatz into the full PDE (2) and separating out orders of δ , we obtain at $\mathcal{O}(1)$ the traveling wave equation (A2) for $k_y = 0$. At $\mathcal{O}(\delta)$ we obtain

$$0 = \mathbb{L}(\Phi_Y U_1) = \Phi_Y \mathbb{L} U_1,$$

as Φ_Y is independent of x. Note this is consistent with (A4) above. Finally, at $\mathcal{O}(\delta^2)$ we obtain

$$\begin{split} \mathrm{i}\Phi_{T}A_{0} - \frac{\omega}{2}\Phi_{Y}^{2}A_{2} &= \mathcal{L}(0)w_{1} + (1 + \mathrm{i}\alpha)\left(\frac{\Phi_{Y}^{2}}{2}\partial_{x}^{2}A_{2} + (\mathrm{i}\Phi_{YY} - \Phi_{Y}^{2})A_{0}\right) + (c\partial_{x} + \chi)\frac{\Phi_{y}^{2}}{2}A_{2} \\ &- (1 + \mathrm{i}\gamma)\left(A_{0}\bar{A}_{0}(A_{2}\Phi_{Y}^{2} + 2w_{1}) + A_{0}^{2}(\bar{A}_{2}\frac{\Phi_{Y}^{2}}{2} + w_{1}) + \frac{\Phi_{Y}^{2}}{2}(2\bar{A}_{0}A_{1}^{2} + 4A_{0}A_{1}\bar{A}_{1})\right) \end{split} \tag{A12}$$

as well as its complex conjugate equation. Rearranging and

using (A6) we then find

$$\mathbb{L}\begin{pmatrix} w_{1} \\ \bar{w}_{1} \end{pmatrix} = -\begin{pmatrix} iA_{0} \left(\Phi_{T} - (1 + i\alpha)(\Phi_{YY} + i\Phi_{Y}^{2}) \right) \\ -iA_{0} \left(\Phi_{T} - (1 - i\alpha)(\Phi_{YY} - i\Phi_{Y}^{2}) \right) \end{pmatrix} + \frac{\Phi_{Y}^{2}}{2} \mathbb{L}U_{2} + \frac{\Phi_{Y}^{2}}{2} D^{2} \mathcal{N}(A_{0}, \bar{A}_{0}) [U_{1}, U_{1}]$$

$$= -\begin{pmatrix} iA_{0} \left(\Phi_{T} - (1 + i\alpha)(\Phi_{YY} + i\Phi_{Y}^{2}) \right) \\ -iA_{0} \left(\Phi_{T} - (1 - i\alpha)(\Phi_{YY} - i\Phi_{Y}^{2}) \right) \end{pmatrix} - \frac{\Phi_{Y}^{2}}{2} \partial_{k_{y}}^{2} \mathcal{L}(0) \begin{pmatrix} A_{0} \\ \bar{A}_{0} \end{pmatrix}$$

$$= -\begin{pmatrix} iA_{0} \left(\Phi_{T} - (1 + i\alpha)(\Phi_{YY} + i\Phi_{Y}^{2}) \right) \\ -iA_{0} \left(\Phi_{T} - (1 - i\alpha)(\Phi_{YY} - i\Phi_{Y}^{2}) \right) \end{pmatrix} + \frac{\Phi_{Y}^{2}}{2} \begin{pmatrix} 2(1 + i\alpha)A_{0} \\ -2(1 - i\alpha)\bar{A}_{0} \end{pmatrix} + \frac{\Phi_{Y}^{2}}{2} \partial_{k_{y}}^{2} \omega_{f}(0) \begin{pmatrix} iA_{0} \\ -iA_{0} \end{pmatrix}. \tag{A13}$$

Using (A9), this can then be simplified to obtain

$$\mathbb{L}\begin{pmatrix} w_1 \\ \bar{w}_1 \end{pmatrix} = -\begin{pmatrix} iA_0 \left(\Phi_T - (1 + i\alpha) \Phi_{YY} \right) \\ -iA_0 \left(\Phi_T - (1 - i\alpha) \Phi_{YY} \right) \end{pmatrix} \\
+ \frac{\Phi_Y^2}{2} \partial_{k_y}^2 \omega_f(0) \begin{pmatrix} iA_0 \\ -iA_0 \end{pmatrix}.$$
(A14)

To solve for (w_1, \bar{w}_1) , the right hand side of must be perpendicular to the adjoint kernel, spanned by $U^{\rm ad}$. Taking the inner product of the right hand side of (A14) with $U^{\rm ad}$ and using the fact that $U_0 = (\mathrm{i}A_0, -\mathrm{i}A_0)^T$ we then obtain

$$\Phi_T = \left\langle \left(\begin{array}{c} i(1+i\alpha)A_0 \\ -i(1-i\alpha)A_0 \end{array} \right), U_{ad} \right\rangle \Phi_{YY} + \frac{\partial_{k_y}^2 \omega_f(0)}{2} \Phi_Y^2.$$
(A15)

Combining this with the computation in (A9), we obtain from (A15) the desired leading order phase modulation equation,

$$\Phi_{T} = \frac{\lambda_{\text{lin}}''(0)}{2} \Phi_{YY} + \frac{\omega_{\text{f}}''(0)}{2} \Phi_{Y}^{2}, \tag{A16}$$

which can be readily differentiated in Y to obtain the equation for the wavenumber modulation given in (9) above.

⁴D. G. Míguez, M. Dolnik, A. P. Muñuzuri, and L. Kramer, "Effect of axial growth on Turing pattern formation," Phys. Rev. Lett. **96**, 048304 (2006).

⁶R. Goh and B. de Rijk, "Spectral stability of pattern-forming fronts in the complex Ginzburg-Landau equation with a quenching mechanism," Non-linearity **35**, 170–244 (2022).

⁷R. Goh, "Quenched stripes: Wavenumber selection and dynamics," SIAM DSWeb (2021).

⁸R. Goh and A. Scheel, "Growing patterns," submitted, arXiv preprint arXiv:2302.13486 (2023).

⁹G. Schneider, "Diffusive stability of spatial periodic solutions of the Swift-Hohenberg equation," Communications in Mathematical Physics **178**, 679–702 (1996).

¹⁰I. S. Aranson and L. Kramer, "The world of the complex Ginzburg-Landau equation," Rev. Mod. Phys. **74**, 99–143 (2002).

¹¹R. Goh and A. Scheel, "Triggered fronts in the complex Ginzburg Landau equation," J. Nonlinear Sci. 24, 117–144 (2014).

¹²W. van Saarloos, "Front propagation into unstable states," Physics Reports

¹³E. J. Doedel, A. R. Champneys, F. Dercole, T. F. Fairgrieve, Y. A. Kuznetsov, B. Oldeman, R. Paffenroth, B. Sandstede, X. Wang, and C. Zhang, "Auto-07p: Continuation and bifurcation software for ordinary differential equations," (2007).

¹⁴A. Doelman, B. Sandstede, A. Scheel, and G. Schneider, "The dynamics of modulated wave trains," Mem. Amer. Math. Soc. 199, viii+105 (2009).

¹⁵A.-K. Kassam and L. N. Trefethen, "Fourth-order time-stepping for stiff PDEs," SIAM Journal on Scientific Computing 26, 1214–1233 (2005).

¹⁶J.-P. Eckmann, T. Gallay, and C. E. Wayne, "Phase slips and the eckhaus instability," Nonlinearity 8, 943 (1995).

¹⁷J. Swift and P. C. Hohenberg, "Hydrodynamic fluctuations at the convective instability," Physical Review A 15, 319 (1977).

¹⁸A. Mielke, "Instability and stability of rolls in the Swift–Hohenberg equation," Communications in Mathematical Physics 189, 829–853 (1997).

¹⁹R. Goh and A. Scheel, "Pattern-forming fronts in a Swift-Hohenberg equation with directional quenching—parallel and oblique stripes," J. Lond. Math. Soc. (2) 98, 104–128 (2018).

²⁰M. Avery, R. Goh, O. Goodloe, A. Milewski, and A. Scheel, "Growing stripes, with and without wrinkles," SIAM Journal on Applied Dynamical Systems 18, 1078–1117 (2019).

²¹E. Gengel and A. Pikovsky, "Phase demodulation with iterative hilbert transform embeddings," Signal Processing 165, 115–127 (2019).

²²T. W. Hiscock and S. G. Megason, "Orientation of Turing-like patterns by morphogen gradients and tissue anisotropies," Cell Systems 1, 408 – 416 (2015).

²³R. Kurita, "Control of pattern formation during phase separation initiated by a propagated trigger," Scientific Reports 7, 6912 (2017).

¹H. Riecke, "Pattern selection by weakly pinning ramps," EPL (Europhysics Letters) **2**, 1 (1986).

²S. Akamatsu, S. Bottin-Rousseau, and G. Faivre, "Experimental evidence for a zigzag bifurcation in bulk lamellar eutectic growth," Phys. Rev. Lett. **93**, 175701 (2004).

³C. Konow, N. H. Somberg, J. Chavez, I. R. Epstein, and M. Dolnik, "Turing patterns on radially growing domains: experiments and simulations," Physical chemistry chemical physics: PCCP 21, 6718—6724 (2019).

⁵M. Avery, R. Goh, O. Goodloe, A. Milewski, and A. Scheel, "Growing stripes, with and without wrinkles," SIAM J. Appl. Dyn. Syst. **18**, 1078–1117 (2019).

- ²⁴E. M. Foard and A. J. Wagner, "Survey of morphologies formed in the wake of an enslaved phase-separation front in two dimensions," Phys. Rev. E 85, 011501 (2012).
- ²⁵D. Double, "Imperfections in lamellar eutectic crystals," Materials Science and Engineering 11, 325 – 335 (1973).
- ²⁶U. Thiele, "Patterned deposition at moving contact lines," Advances in Colloid and Interface Science 206, 399 413 (2014), manuel G. Velarde.
- ²⁷L. N. Howard and N. Kopell, "Slowly varying waves and shock structures in reaction-diffusion equations," Studies in Applied Mathematics 56, 95–145 (1977), https://onlinelibrary.wiley.com/doi/pdf/10.1002/sapm197756295.
- ²⁸T. Passot and A. C. Newell, "Towards a universal theory for natural patterns," Physica D: Nonlinear Phenomena 74, 301–352 (1994).
- ²⁹N. M. Ercolani, R. Indik, A. C. Newell, and T. Passot, "The geometry of the phase diffusion equation," Journal of Nonlinear Science 10, 223–274 (2000).
- ³⁰B. A. Malomed, A. A. Nepomnyashchy, and M. I. Tribelsky, "Domain

- boundaries in convection patterns," Physical Review A 42, 7244 (1990).
- ³¹K. Chen, Z. Deiman, R. Goh, S. Jankovic, and A. Scheel, "Strain and defects in oblique stripe growth," Multiscale Modeling & Simulation 19, 1236–1260 (2021).
- ³²A. J. Bernoff, "Slowly varying fully nonlinear wavetrains in the Ginzburg-Landau equation," Physica D: Nonlinear Phenomena 30, 363–381 (1988).
- ³³V. Biktashev, "Diffusion of autowaves: Evolution equation for slowly varying autowaves," Physica D: Nonlinear Phenomena 40, 83–90 (1989).
- ³⁴Y. Kuramoto, *Chemical turbulence* (Springer, 1984).
- ³⁵M. C. Cross and P. C. Hohenberg, "Pattern formation outside of equilibrium," Rev. Mod. Phys. 65, 851–1112 (1993).
- ³⁶Y. Masutomi and K. Nozaki, "Derivation of non-isotropic phase equations from a general reaction-diffusion equation," Physica D: Nonlinear Phenomena 151, 44–60 (2001).